Interaction of Toposome from Sea-Urchin Yolk Granules with Dimyristoyl Phosphatidylserine Model Membranes: A ^{2}H-NMR Study

Michael Hayley,* Jason Emberley,† Philip J. Davis,* Michael R. Morrow,† and John J. Robinson*
*Department of Biochemistry, and †Department of Physics and Physical Oceanography, Memorial University of Newfoundland, St. John's, Newfoundland, Canada

ABSTRACT The yolk granule is the most abundant membrane-bound organelle present in sea urchin eggs and embryos. The major protein component of this organelle, toposome, accounts for ~50% of the total yolk protein and has been shown to be localized to the embryonic cell surface. Extensive characterization in several laboratories has defined a role for toposome in mediating membrane-membrane interactions. The current study expands the analysis of toposome-membrane interaction by defining toposome-induced changes to the lipid bilayer. The effect of toposome on the biophysical properties of phosphatidyl serine (PS) multibilayers was investigated using deuterium nuclear magnetic resonance and perdeuterated dimyristoyl PS (DMPS-d_{54}). Toposome was found to have little effect on DMPS-d_{54} chain orientational order in both the gel and liquid-crystalline phases. Timescales for DMPS-d_{54} reorientation were investigated using quadropole echo decay. Echo decay times were sensitive to toposome in the liquid-crystalline phase but not in the gel phase. Additional information about the perturbation of bilayer motions by toposome was obtained by analyzing its effect on the decay of Carr-Purcell-Meiboom-Gill echo trains. Collectively, these results suggest that toposome interacts peripherally with DMPS bilayers and that it increases the amplitude of lipid reorientation, possibly through local enhancement of bilayer curvature.

INTRODUCTION

Evenly distributed throughout the cytoplasm, yolk granules occupy approximately one-third of the cytoplasmic volume and are present in the eggs, embryos and early larvae of the sea urchin. Yolk proteins, ranging in size from 35 to 300 kDa, account for 10–15% of the total egg protein (1–4). Toposome represents ~50% of the total yolk protein and is the major protein component of this organelle (5). First discovered by Malkin and co-workers (6), toposome was initially isolated from the sea urchin embryo in studies aimed at identifying molecules responsible for cell-cell adhesion (7,8).

In the sea urchin *Strongylocentrotus purpuratus*, toposome appears to be a hexameric glycoprotein consisting of six identical subunits, each of 160 kDa. The hexamer is characterized by intrachain disulfide bonds and is stabilized with calcium. In the absence of this cation, the hexamer dissociates into trimer, dimer, and monomer forms (7). The functional unit(s) remains to be determined. In addition to the yolk granule, toposome is also localized to the embryonic cell surface and has been identified as a molecule mediating cell-cell adhesion in the developing embryo (7,8). Interestingly, as development proceeds, the 160-kDa polypeptide is proteolytically processed into species of smaller molecular mass. This processing is dependent upon a thiol-class protease associated with the yolk granule and commences within 6 h after fertilization. The functional significance of this processing remains to be determined.

We have previously characterized toposome-driven membrane-membrane interactions using both liposomes and purified yolk granules (9). This earlier work has recently been extended by an analysis of calcium-toposome interaction. This cation was found to induce two calcium-concentration-dependent structural transitions in toposome: a secondary structural change occurred with an apparent k_d (calcium) of 25 μM and this was followed by a tertiary structural change with an apparent k_d (calcium) of 240 μM (10). Interestingly, the first structural change was required to facilitate toposome binding to bilayers, whereas the second structural change correlated with toposome-driven membrane-membrane interaction. These results provide a structural basis for the previously described toposome-mediated cell-cell adhesion in the sea urchin embryo.

Quantitatively, the yolk granule organelle represents a significant intracellular store of both membrane and protein and, as such, has been the subject of extensive research. However, although the constituent elements of this organelle have been identified and characterized, its function remains uncertain. Classically, this organelle has been viewed as a reservoir of nutrients for the developing embryo. However, recent work suggests that the yolk granules remain intact throughout the course of embryonic development and are only metabolized in 7-day-old larvae (11). In addition, when larvae are starved, their yolk-granule content remains unchanged. Data from several laboratories suggest a more dynamic role for the yolk granule in the developing embryo. A number of reports have described the localization to the yolk granule of proteins destined for subsequent export to the

Submitted May 25, 2006, and accepted for publication September 7, 2006.

Address reprint requests to John J. Robinson, Dept. of Biochemistry, Memorial University of Newfoundland, St. John's, Newfoundland, A1B 3X9 Canada. Tel.: 709-737-8545; Fax: 709-737-2422; E-mail: johnro@mun.ca.

0006-3495/06/12/4555/10 $2.00

doi: 10.1529/biophysj.106.089979

extracellular environment (12,13). In addition, the large amount of membrane associated with the yolk granule may serve as a reservoir for patching lesions in the plasma membrane of sea urchin eggs and embryos (14,15). The association of toposome with the yolk granule may equip this organelle with the capacity to engage in processes requiring dynamic membrane-membrane interactions.

The primary objective of this study was to investigate whether the interaction of toposome with the bilayer is more characteristic of a peripheral protein, with protein-lipid interactions primarily at the bilayer surface, or of an integral protein extending partly into or spanning the lipid bilayer. Toposome-bilayer interactions were examined in the presence of calcium concentrations known to induce either the secondary structural change in toposome or both the secondary and tertiary structural changes. ^{2}H-NMR was used to monitor the effect of toposome on lipid acyl-chain orientational order and bilayer motions in gel and liquid-crystalline 1,2,-perdeuterodimyristoyl-*sn*-glycero-3-phosphoserine (DMPS-d_{54}) model membranes. DMPS-d_{54} acyl-chain orientational order was examined using chain deuteron quadrupole splitting and first spectral moments. Information regarding the perturbation of bilayer motion by toposome was inferred from the effects of the protein on characteristic decay times for chain deuteron quadrupole echoes and Carr-Purcell-Meiboom-Gill echo trains.

MATERIALS AND METHODS

Chain-perdeuterated DMPS-d_{54} was obtained from Avanti Polar Lipids (Alabaster, AL) and used without further purification. Toposome was purified from the sea urchin *Strongylocentrotus purpuratus* purchased from SeaCology (Vancouver, British Columbia, Canada). Eggs were harvested and washed consecutively in Millipore-filtered sea water and Ca^{2+}, Mg^{2+}-free sea water. Preparation of the yolk granule protein extracts was based on a procedure described previously (9), but with some modifications. Washed eggs were suspended in 0.5 M KCl (pH 7.0) in the presence of EDTA (ethylenediamine tetraacetic acid) and homogenized in a hand-held Dounce homogenizer at 0°C. The homogenate was then fractionated by centrifugation at 400 × *g* for 4 min at 4°C. The supernant then underwent fractionation by centrifugation at 2400 × *g* for 10 min at 4°C. The final pellet was resuspended in 0.5 M KCl (pH 7.0) in the presence of 1 mM EDTA, after which it was fractionated by centrifugation at 50,000 × *g* for 1 h at 4°C and the supernatant retained. Aliquots of the supernant were dialyzed against starting buffer (10 mM Tris-HCl, pH 8.0) and were loaded onto a Q-Sepharose Fast Flow column (Amersham Pharmacia, Uppsala, Sweden) that had been previously equilibrated with starting buffer. The column was washed three times to remove any unbound proteins, followed by the elution of bound proteins with a NaCl step gradient (0.1–1.0 M), prepared in starting buffer. The eluted proteins were analyzed by sodium dodecyl sulfate polyacrylamide gel electrophoresis as described by Laemmli (16), and the gel was stained with silver (Amersham Pharmacia). The salt fraction containing the purified toposome was stored in small aliquots at −20°C.

Multilamellar vesicles used in the ^{2}H-NMR study were prepared using two different protocols. DMPS-d_{54} was hydrated at 45°C for 1 h in deuterium-depleted buffer (20 mM Tris-HCl, 150 mM NaCl, pH 8.0) containing both toposome and calcium. In one preparation, using a lipid: protein ratio of 80,000:1, DMPS-d_{54} was dissolved in deuterium-depleted buffer (20 mM Tris-HCl, 150 mM NaCl, pH 8.0) and hydrated at 45°C for 1 h. Toposome and calcium were then added to the preformed multilamellar vesicles. In both protocols, samples were transferred to NMR tubes, and each sample contained 5 mg of DMPS-d_{54}. In parallel experiments, the final lipid/protein ratios in the reconstituted samples were determined after the isolation, by centrifugation, of the liposomal pellets.

Wideline deuterium NMR spectra and echo-decay measurements were obtained with a locally constructed spectrometer using quadrupole echo pulse sequences (17). For all acquisitions, a repetition time of 0.5 s was used. Free induction decays used to obtain spectra of samples of DMPS-d_{54} were obtained in a 9.4-T superconducting solenoid using the quadrupole echo sequence with $\pi/2$ pulses of 5.0–5.5 μs separated by 35 μs. Typically, 20,000 transients were averaged for each spectrum. Signals were obtained using oversampling (18) and digitized with effective dwell times of 4 μs for liquid crystal DMPS-d_{54} spectra and 2 μs for gel DMPS-d_{54} spectra. Spectrometer frequency and pulse lengths were adjusted before acquisition to minimize signal in the imaginary channel. No line broadening was used. Spectra that would correspond to samples with bilayer normals aligned perpendicular to the applied magnetic field were obtained by transforming the multilamellar vesicle spectra using a fast Fourier-transform ''de-Pakeing'' algorithm (19).

Quadrupole echo amplitudes for determination of quadrupole echo decay times were recorded by averaging 2000–4000 transients. Decays were plotted as $\ln(A(2\tau))$ versus 2τ and average echo decay times, T_{2e}, were obtained from the inverse slope of the initial decay.

Bloom and Sternin (20) pioneered use of the quadrupole Carr-Purcell-Meiboom-Gill (q-CPMG) pulse sequence $[(\pi/2)_x - (\pi/2)_y - (\pi/2)_n]$ for identification of contributions to quadrupole echo decay from motions with correlation times that are too long to contribute to motional narrowing of spectra. This sequence results in the formation of echoes at multiples of 2τ. Decay of the echo train is less sensitive to motions that modulate the quadrupole interaction with correlation times much longer than τ. By observing the decay of q-CPMG echo decay trains for progressively larger values of τ., it is possible to reintroduce contributions to echo train decay from progressively slower motions and probe the distribution of such motions. In this work, q-CPMG echo trains were recorded for $\tau = 40\,\mu$s, $\tau = 50\,\mu$s, $\tau = 100\,\mu$s, $\tau = 150\,\mu$s, $\tau = 200\,\mu$s, $\tau = 300\,\mu$s, $\tau = 400\,\mu$s, and $\tau = 500\,\mu$s. For $\tau \leq 100\,\mu$s, 40 echoes were recorded in each train. For larger values of τ, the maximum number of echoes recorded in an echo train was determined by the condition $2n_{max}\tau \leq 8$ ms. Echo amplitudes were measured from averages of 4000 acquisitions of each echo train.

As described below, q-CPMG results were fitted to a model for the distribution of motions in a sample by simultaneously minimizing squares of differences between modeled and observed echo amplitudes (χ^2) for all echo-train decays in a given experiment. This fitting was carried out using the multiple data set fitting capability of Origin 6.1 (Originlab, Northhampton, MA). The fit was applied simultaneously to the eight echo-train decay data sets for a given sample. Except for the value of τ. specific to each echo-train decay, all parameters in the fit were designated as shared by all data sets. The resulting fits reflect the adjustment of nine variables to fit, simultaneously, eight nonexponential decay curves.

RESULTS AND DISCUSSION

Toposome was purified using the standard protocol described in Materials and Methods. Analysis by reduced SDS-PAGE revealed that the protein was homogenous. We have previously characterized both the effects of calcium on toposome structure and toposome-driven membrane-membrane adhesion (9,10). The calcium concentration used in the NMR study reported here, as well as the lipid/protein ratios in the toposome-reconstituted liposomes were chosen based on our previous studies noted above. Therefore, the conditions chosen for this study are those that allow for both reconstitution of toposome with the liposomal bilayer and

the demonstration of the known biological activity of toposome.

Fig. 1 shows ^{2}H NMR spectra at selected temperatures for (*A*) DMPS-d_{54}, (*B*) DMPS-d_{54} plus calcium (100 μM), and (*C*) DMPS-d_{54} plus calcium (100 μM) and toposome (lipid/protein ratio 80,000:1). The sample from which the spectra in Fig. 1 *C* were obtained was prepared by adding toposome to preformed multilamellar vesicles. We have previously shown that toposome binds to phosphatidyl serine liposomes in a calcium-dependent manner with an apparent k_d (calcium) of 25 μM (10). At temperatures above 31°C, all the spectra in Fig. 1, are characteristic of lipid in the liquid-crystalline phase. The spectra are superpositions of Pake doublets that are indicative of axially symmetric CD bond reorientations that modulate the quadrupole interaction with correlation times that are short relative to the characteristic timescale ($\sim 10^{-5}$ s) of the ^{2}H-NMR measurement (21). The distribution of quadrupole splittings reflects the dependence of CD bond orientational order on position along the perdeuterated acyl chains (21). Below 32°C, the broader and more continuous spectra are characteristic of the gel phase. This reflects lipid reorientational dynamics that are slower and reorientation that is less axially symmetric on the timescale of the measurement. In all samples studied, the transition from liquid-crystal to gel phase proceeded sharply and none of the observed spectra displayed superpositions of liquid-crystal- and gel-phase features that would be indicative of two-phase coexistence.

Comparison of the three series of spectra in Fig. 1 suggests that addition of calcium and then toposome at a lipid/protein molar ratio of 80,000:1 has little apparent effect on either the bilayer phase transition or lipid acyl chain orientational order in the liquid-crystalline phase. The insensitivity of chain deuteron quadrupole splitting to toposome is illustrated in Fig. 2, which compares the right halves of de-Paked spectra at 40°C for DMPS-d_{54} alone (*A*) and in the presence of toposome (lipid/protein molar ratio 80,000:1) and calcium (100 μM) (*B*). The spectra shown were obtained by transforming the corresponding unoriented-sample spectra from Fig. 1 to obtain spectra that would be expected from samples with bilayers uniformly oriented perpendicular to the magnetic field. The vertical lines between the spectra are centered on the peaks of the upper spectrum to aid in comparison of quadrupole splittings of resolvable doublets. This comparison indicates that at a lipid/protein molar ratio of 80,000:1, toposome, in the presence of sufficient calcium to allow its association with the bilayer, does not significantly alter DMPS-d_{54} deuteron quadrupole splittings. This result indicates that toposome does not significantly alter the amplitudes of fast fatty acyl chain motions and suggests a peripheral association of toposome with the bilayer.

A series of DMPS-d_{54}/protein mixtures were also prepared by hydrating the lipid in buffer containing the protein plus calcium. These preparations most likely contain protein and calcium homogenously distributed throughout the multilamellar membrane surfaces. Fig. 3 shows NMR spectra at selected temperatures for DMPS-d_{54} plus toposome at three lipid/protein molar ratios (80,000:1, 30,000:1, and 15,000:1) in the presence of either 100 or 500 μM Ca^{2+}. The spectra

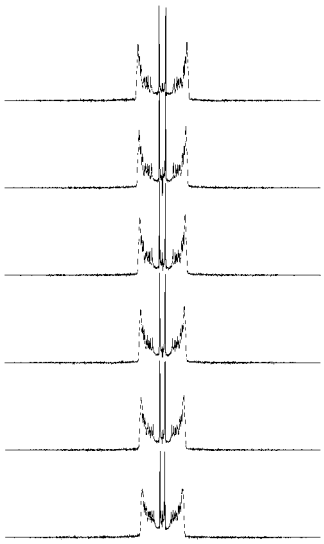

FIGURE 1 ^{2}H NMR spectra at selected temperatures for (*A*) DMPS-d_{54}, (*B*) DMPS-d_{54} plus calcium (100 μM Ca^{2+}), and (*C*) DMPS-d_{54} plus Ca^{2+} (100 μM) and toposome (lipid/protein ratio 80,000:1). For each series of spectra, a single sample was analyzed.

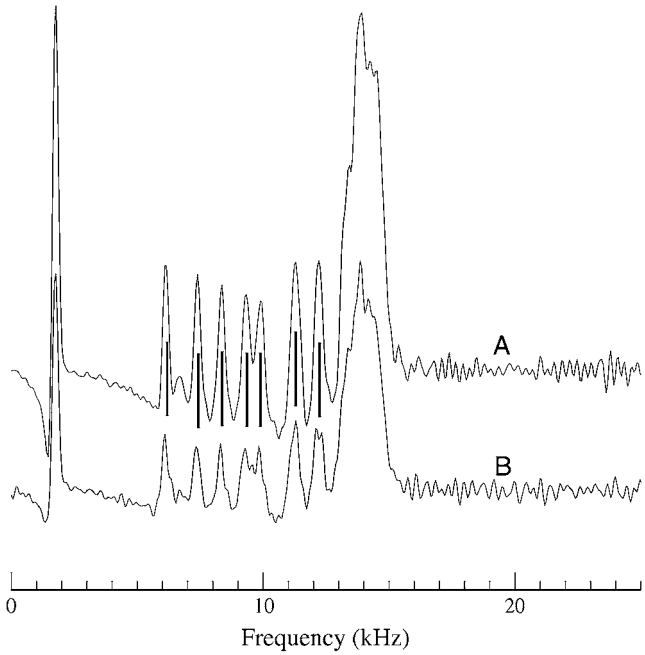

FIGURE 2 Depaked spectra (*right halves*) at 40°C for (*A*) DMPS-d_{54} and (*B*) DMPS-d_{54} in the presence of Ca^{2+} (100 μM) and toposome at a lipid/protein ratio of 80,000:1. Spectra are obtained by transforming unoriented-sample spectra to obtain spectra that would be expected from bilayers oriented with the bilayer normal perpendicular to the applied field.

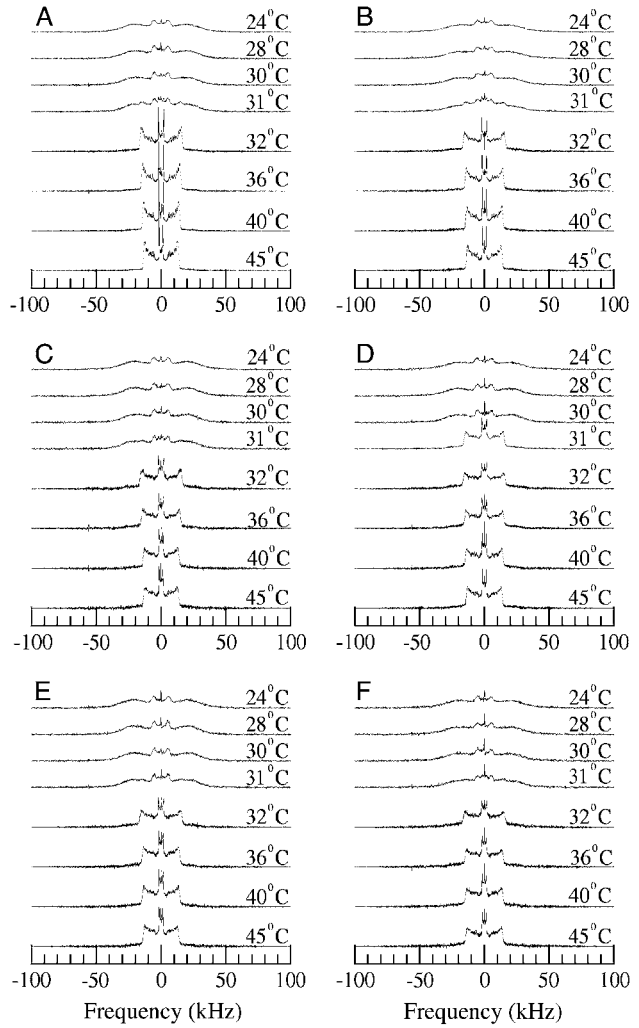

FIGURE 3 ^{2}H NMR spectra at selected temperatures for DMPS-d_{54} plus toposome and calcium. (*A*, *C*, and *E*) Spectra in which the lipid/protein ratios were 80,000:1, 30,000:1, and 15,000:1, respectively, in 100 μM Ca^{2+}. (*B*, *D*, and *F*) Spectra in which the lipid/protein ratios were 80,000:1, 30,000:1, and 15,000:1, respectively, in 500 μM Ca^{2+}. For each series of spectra, a single sample was analyzed.

for liposomes (lipid/protein ratio 80,000:1) prepared in this way are effectively identical to those obtained from corresponding samples prepared by adding toposome to preformed multilamellar vesicles (compare Figs. 1 *C* and 3 *A*). For a given temperature, deuteron splittings in the liquid crystalline spectra decrease only slightly with increasing protein concentration. This observation indicates that increased protein concentration has little effect on lipid chain packing within the bilayer. The liquid-crystal-to-gel transition remains sharp at all protein concentrations. Increasing protein concentration does affect the signal/noise ratio and the resolution of superimposed doublets in the liquid-crystalline spectra. This reflects changes in the echo decay rate with protein concentration, as described below.

For a symmetric spectrum $s(\omega)$, the first spectral moment, defined as

$$M_1 = \frac{\int_0^\infty \omega s(\omega) d\omega}{\int_0^\infty s(\omega) d\omega}, \quad (1)$$

is proportional to the intensity-weighted average, over all deuterons, of the quadrupole-splitting. Values of M_1 thus reflect the average orientational order of chain-perdeuterated lipid bilayers. Fig. 4 shows the temperature dependence of M_1 for the spectra of DMPS-d_{54}, DMPS-d_{54} in the presence of 100 μM Ca^{2+}, DMPS-d_{54} in the presence of 100 μM Ca^{2+} and toposome at three lipid to protein molar ratios (80,000:1 (*open up* and *down triangles*), 30,000:1 (*open square*), and 15,000:1 (×)), and DMPS-d_{54} in the presence of 500 μM Ca^{2+} and toposome at three lipid/protein molar ratios (80,000:1 (*open side triangle*), 30,000:1 (*open diamond*), and 15,000:1 (*cross*)). In the liquid-crystalline phase, toposome in the presence of Ca^{2+} reduces average chain orientational order slightly. This reduction in chain order, although small, does appear to depend on the lipid/protein molar ratio; however, there does not appear to be any significant difference between the effects of toposome in the presence of Ca^{2+} at 100 μM or 500 μM, indicating that the

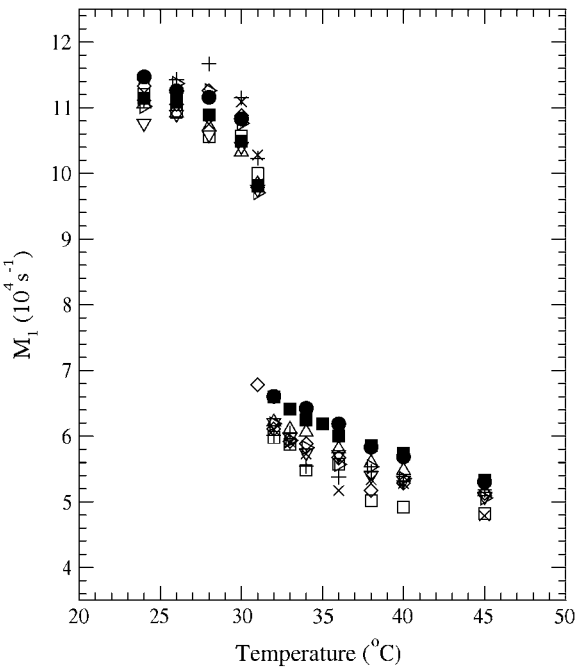

FIGURE 4 Temperature dependence of first spectral moments (M_1) for the spectra in Figs. 1 and 3. DMPS-d_{54} (●), DMPS-d_{54} plus 100 μM Ca^{2+} (■); two preparations of DMPS-d_{54} plus toposome (lipid/protein = 80,000:1) in 100 μM Ca^{2+} (△ and ▽); DMPS-d_{54} plus toposome (lipid/protein = 80,000:1) in 500 μM Ca^{2+} (▷); DMPS-d_{54} plus toposome (lipid/protein = 30,000:1) in 100 μM Ca^{2+} (□); DMPS-d_{54} plus toposome (lipid/protein = 30,000:1) in 500 μM Ca^{2+} (◇); DMPS-d_{54} plus toposome (lipid/protein = 15,000:1) in 100 μM Ca^{2+} (×); DMPS-d_{54} plus toposome (lipid/protein = 15,000:1) in 500 μM Ca^{2+} (+).

tertiary structural change induced by the higher concentration of calcium does not result in any additional modulation of toposome-membrane interactions. Any dependence of M_1 on toposome concentration in the gel phase is smaller than the scatter in that data. Despite scatter in the M_1 data in both phases, it is clear that toposome in the presence of calcium has little effect on the DMPS-d_{54} liquid-crystal-to-gel-phase transition. This result confirms the absence of any significant effect of toposome on the amplitudes of rapid motions of the fatty acyl chains and again points to a peripheral association of toposome.

Protein-membrane interactions, which have little effect on chain order, may still perturb bilayer motions that are sensitive to reorientation on the 10^{-5}- to 10^{-4}-s timescale. Quadrupole echo decay measurements can be utilized to detect these perturbations. The quadrupole echo pulse sequence consists of two $\pi/2$ pulses differing in phase by 90° and separated by an interval τ (17). Motions that change the quadrupole interaction while an echo is being formed contribute to echo decay. For motions that have short correlation times (τ_c) relative to the inverse spectral width, the contribution to the echo decay rate is proportional to (τ_c) (22). For slower motions, the contribution to the echo decay rate is proportional to τ_C^{-1} (23). Slow diffusive or collective motions and faster local motions can both contribute to echo decay in the liquid-crystalline phase (20,24,25). In this phase, motions that contribute to echo decay include slower motions such as collective modes of the bilayer surface and molecular reorientation resulting from diffusion of molecules around curved bilayer surfaces, as well as faster, more localized motions including molecular reorientation and conformational fluctuations (20,25–27). At the liquid-crystal-to-gel transition, the correlation times for slow motions, such as lateral diffusion and collective motions (membrane undulations), increase and their contributions to echo decay are consequently reduced. In contrast, motions that are fast in the liquid-crystalline phase, such as reorientation about the bilayer normal, can slow at the transition and contribute more effectively to echo decay. The result is a sharp drop in the echo decay time at the liquid-crystal-to-gel transition. As the temperature is lowered further in the gel phase, the more localized motions begin to freeze out, thus becoming less effective contributors to echo decay, and T_{2e} increases.

Fig. 5 shows echo decay times at selected temperatures for DMPS-d_{54} (*solid circle*), DMPS-d_{54} in the presence of 100 μM Ca^{2+} (*solid square*), and DMPS-d_{54} in the presence of 100 μM Ca^{2+} plus toposome at three lipid/protein molar ratios (80,000:1 (*open up* and *down triangles*), 30,000:1 (*open square*), and 15,000:1 (×)). DMPS-d_{54} in the presence of 500 μM Ca^{2+} at three lipid/protein molar ratios 80,000:1 (open *side triangle*), 30,000:1 (*open diamond*), and 15,000:1 (*cross*)) was also studied. In the liquid-crystalline phase (>32°C), addition of toposome at a lipid/protein molar ratio of 80,000:1 increases the quadrupole echo decay rate significantly, as reflected by the reduced values for T_{2e}. Decreasing

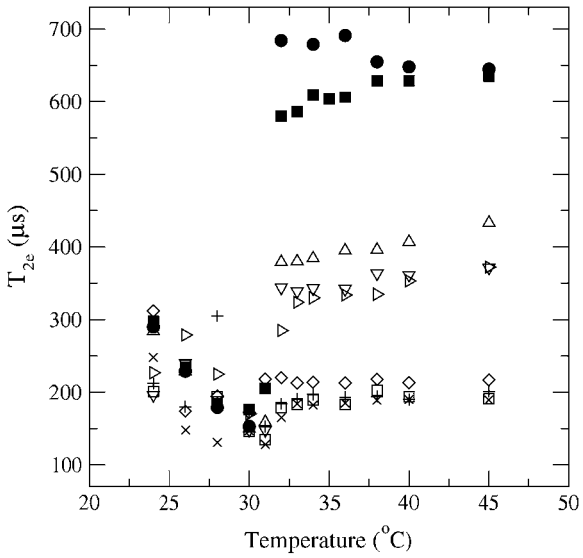

FIGURE 5 Temperature dependence of average quadrupole echo decay time (T_{2e}) extracted from Figs. 1 and 3. DMPS-d_{54} (●); DMPS-d_{54} plus 100 μM Ca^{2+} (■); two preparations of DMPS-d_{54} plus toposome (lipid/protein = 80,000:1) in 100 μM Ca^{2+} (△and ▽); DMPS-d_{54} plus toposome (lipid/protein = 80,000:1) in 500 μM Ca^{2+} (▷); DMPS-d_{54} plus toposome (lipid/protein = 30,000:1) in 100 μM Ca^{2+} (■); DMPS-d_{54} plus toposome (lipid/protein = 30,000:1) in 500 μM Ca^{2+} (◇); DMPS-d_{54} plus toposome (lipid/protein = 15,000:1) in 100 μM Ca^{2+} (×); DMPS-d_{54} plus toposome (lipid/protein = 15,000:1) in 500 μM Ca^{2+} (+).

the lipid/protein molar ratio to 30,000:1 increases the quadrupole echo decay rate even further as shown by a more dramatic fall in the T_{2e}-values. No further change in T_{2e}-values was observed when the lipid/protein molar ratio was decreased below 30,000:1. Interestingly, the magnitude of the T_{2e} changes was similar in the presence of either 100 or 500 μM Ca^{2+}.

The effect of toposome on quadrupole echo decay rate in the liquid-crystal phase is much more pronounced than its effect on average chain orientational order over the same temperature range. Chain orientational order reflects averaging of the quadrupole interaction on timescales that are short relative to the characteristic time ($\sim 10^{-5}$ s) for the NMR observation. Therefore, it is likely that the observed effect of toposome on quadrupole echo decay in the liquid-crystalline phase reflects perturbation of diffusive or collective motions (membrane undulations) with longer correlation times, rather than the faster local motions that influence orientational order parameters for each segment. This suggests that toposome may modulate the rate or path of diffusion of phospholipid molecules, which in turn may alter the dynamics of membrane undulations.

In principle, a systematic protein-induced reduction in vesicle radius might account for the observed reduction in liquid-crystal phase quadrupole echo decay time with increasing toposome concentration. However, it is interesting that the change in echo decay time due to the presence of toposome at a lipid/protein ratio of 80,000:1 is not sensitive

to whether toposome is added to preformed multilamellar vesicles or vesicles are formed by hydration of lipid in buffer containing protein (Fig. 5, *open triangles*). This observation does not explicitly preclude a systematic decrease in average vesicle radius with increasing protein concentration. Nevertheless, such an explanation would imply that the addition of protein to preformed multilamellar vesicles promotes substantial reorganization of multilamellar material into vesicles of the same average size as those resulting when vesicles are formed by hydration in buffer containing protein, and that such reorganization does not substantially perturb lipid chain order. An explanation involving more local perturbations of bilayer surface curvature and the spectrum of bilayer surface undulations seems more likely.

Below the liquid-crystal-to-gel-phase transition, quadrupole echo decay times increase slightly with decreasing temperature. However, this effect was independent of the lipid/protein molar ratio. Motions that are slow in the liquid-crystalline phase are generally even slower at low temperature and are not expected to contribute significantly to quadrupole echo decay as the bilayer becomes more ordered. Rotations about the bilayer normal, or about individual bonds, that are fast in the liquid-crystalline phase can slow, on cooling, into the regime where their contributions to the echo decay rate are inversely proportional to their correlation times. Quadrupole echo decay times in the gel phase are thus generally expected to increase with decreasing temperature.

Integral membrane proteins have a tendency to reduce the rate at which echo decay time increases with decreasing temperature in the gel phase. This may reflect a protein-induced interference with ordering and a consequent reduction in temperature-dependent slowing of motions that contribute to quadrupole echo decay in the gel phase (28, 29). The apparent absence of a significant perturbation of quadrupole echo decay rate by toposome in the gel phase suggests that its interaction with the bilayer primarily perturbs motions, such as bilayer undulation and collective motion, that contribute significantly to echo decay in the liquid-crystalline phase but not in the gel phase. Taken along with the relatively weak perturbation of chain orientational order, the echo-decay observations suggest that toposome is not integral to the membrane but interacts primarily at the bilayer surface.

Additional information regarding the nature of the perturbation by toposome can be obtained from multiple pulse experiments. Adiabatic motions are motions that contribute to the quadrupole echo decay but have correlation times that are too long for them to contribute to the motional narrowing of the spectra. Bloom and Sternin (20) demonstrated that the q-CPMG pulse sequence could be used to assess the relative contribution to quadrupole echo decay from slow adiabatic motions for a given sample.

For deuterons whose quadrupole interaction is modulated by a given superposition of motions, the train of echoes formed by the q-CPMG sequence at times $2n\tau$ decays with a rate that is the sum of contributions from each of the motions. The extent to which a given motion i modulates the quadrupole Hamiltonian can be characterized by the second moment of that modulation, ΔM_{2i}. If the correlation time for that motion is τ_{Ci}, then the contribution to the decay rate of the q-CPMG echo train is

$$R_i = \Delta M_{2i}\tau_{Ci}\left[1 - \frac{\tau_{Ci}}{\tau}\tanh\left(\frac{\tau}{\tau_{Ci}}\right)\right], \qquad (2)$$

where 2τ is the separation of echoes in the q-CPMG echo train (20,26,30) . The effect of the factor in square brackets is to substantially reduce the contribution to q-CPMG echo train decay from motions with $\tau_{Ci} \gg \tau$. Varying the pulse spacing from short to long progressively reintroduces the effect of motions with longer correlation times and thus probes the distribution of slower bilayer motions in a sample.

Fig. 6 shows q-CPMG echo-train decays at 38°C for DMPS-d_{54} alone and in the presence of 100 μM Ca^{2+} and toposome at a lipid/protein molar ratio of 80,000:1. Echo trains were collected for $40\,\mu s \le \tau \le 500\mu s$. The echo-train decays are plotted as $\ln(A(2n\tau)/A(2\tau_{min}))$ versus $2n\tau$ where $A(2n\tau)$ is the amplitude of a particular echo and $A(2\tau_{min})$ is the amplitude of the first echo for the experiment using the shortest τ (40 μs for this work). The strongly nonexponential echo-train decays, particularly for larger values of τ, are typical of multilamellar vesicle samples and are similar to previous observations on chain-perdeuterated lipid samples (20,31). The results shown in Fig. 6, for both samples, are characterized by rapid initial decays of increasing fractions of the signal with increasing τ coupled with similar limiting rates of echo-train decay at large $2n\tau$ for all values of τ. The limiting rates at large $2n\tau$ reflect fast, presumably local, motions that modulate the quadrupole interaction of all deuterons in a given sample. The vertical spread of the limiting decay curves suggests that deuteron quadrupole interactions are also modulated by slower motions whose contributions to echo-train decay are sensitive to τ and that different populations of deuterons are affected by slow motions with different correlation times. The presence of toposome results in a faster initial decay of the echo-train signal for all values of τ, but does not significantly alter the vertical separation of limiting decays for a given pair of τ-values.

The τ-dependence of the echo-train decays can be understood as follows. For short τ, only a small fraction of the deuterons are affected by slow motions that are nevertheless fast enough to contribute to echo-train decay for that value of τ. The small portion of the signal from this fraction decays rapidly. The remaining deuterons are affected by slow motions with longer correlation times that do not contribute to echo-train decay for this value of τ and the slow decay of signal from these populations is due to the fast common motion. As τ is increased, the fraction of the sample with slow motions that can contribute significantly to echo-train decay increases. For each value of τ, the signal from this fraction of the sample decays rapidly, leaving the signal from

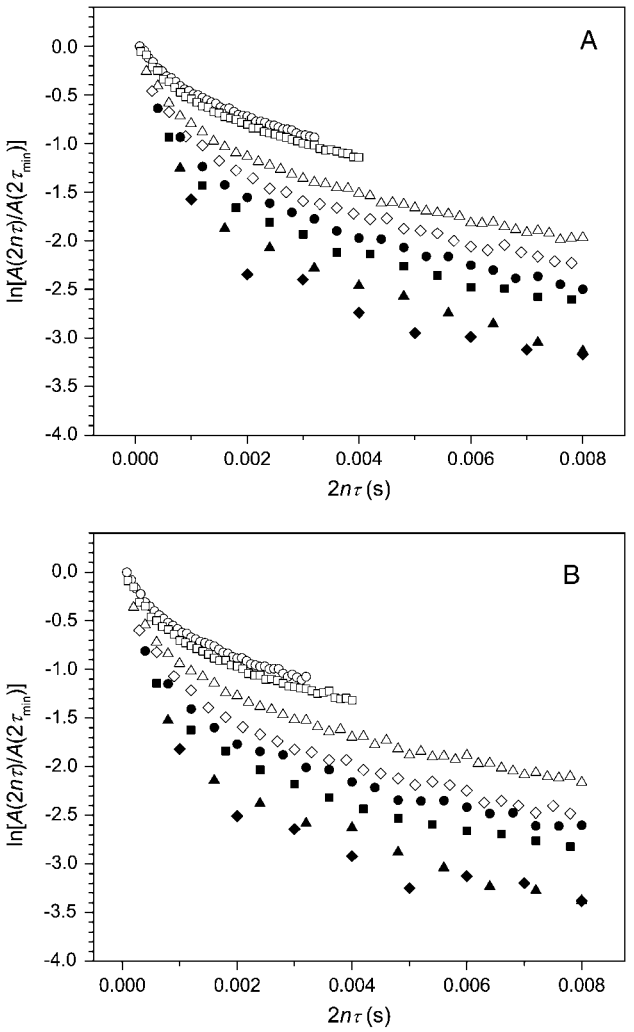

FIGURE 6 Quadrupole Carr-Purcell_Meiboom-Gill echo-train decays for (*A*) DMPS-d_{54} and (*B*) DMPS-d_{54} plus toposome (lipid/protein = 80,000:1) in 100 μM Ca^{2+}. Decays are plotted as $\ln[A(2n\tau)/A(2\tau_{min})]$ versus $2n\tau$, where $A(2n\tau)$ is the amplitude of the n^{th} echo in the train collected with echoes separated by 2τ, and $A(\tau_{min})$ is the amplitude of the first echo obtained with the shortest value of τ. Echo trains were recorded for $\tau = 40\,\mu$s (○);$\tau = 50\,\mu$s(□);$\tau = 100\,\mu$s(8); $\tau = 150\,\mu$s(◇); $\tau = 200\,\mu$s(●); $\tau = 300\,\mu$s (■); $\tau = 400\,\mu$s (▲); and $\tau = 500\,\mu$s(♦). q-CPMG analysis was performed on single samples of either DMPS-d_{54} or DMPS-d_{54} plus toposome (80,000:1 and 100 μM Ca^{2+}).

the rest of the sample to decay at the rate characteristic of fast common motions.

The q-CPMG echoes in multilamellar samples of chain perdeuterated lipids are sums of signals from populations of deuterons in which the quadrupole interaction is modulated to different extents by different superpositions of slow and fast motions. Although the contribution from slow motions covering a wide and effectively continuous range of correlation times precludes precise characterization of the relevant slow motions, the nonexponential character and τ-dependence of the decays can be reproduced using models that approximate the actual spectrum of slow motions by a small number of discrete slow motions. Observing how the parameters of such a model must change to reproduce observed differences between q-CPMG observations on two samples can provide some indication as to the extent to which the changes reflect either a change in the effective spectrum of slow motion correlation times or a change in the amplitudes of such motions.

The simplest model that can reproduce the τ-dependence of the nonexponential decays observed in multilamellar vesicle samples is one in which the quadrupole interaction of each deuteron is modulated by a superposition of one fast and one slow motion (31). The fast motion is assumed to be common to the entire sample and results in a contribution to the echo-train decay rate of $1/T_2'$. A particular slow motion, denoted *i*, is assumed to be specific to particular population of magnitude A_i. For an echo-train decay collected with a particular value of τ, the amplitude of the n^{th} echo can then be written as (31)

$$A(2n\tau) = \sum_{i}^{N} A_i \exp\left(-2n\tau\left\{\Delta M_{2i}\tau_{Ci}\left[1 - \frac{\tau_{Ci}}{\tau}\tanh\left(\frac{\tau}{\tau_{Ci}}\right)\right] + \frac{1}{T_2'}\right\}\right), \quad (3)$$

where τ_{Ci} is the correlation time of motion *i* and ΔM_{2i} is the second moment of the portion of the quadrupole interaction modulated by motion *i*. The sum over populations in Eq. 3 thus approximates what is likely a more continuous distribution of slow motions within a given sample.

The echo-train decays of Fig. 6 were fit to a model based on Eq. 3. The amplitude of the free induction decay following the initial pulse is generally not observable in wideline ^{2}H-NMR experiments because of the finite time required for preamplifier recovery after that pulse. To fit the initial decay of the q-CPMG echo train, though, it is necessary to estimate the amplitude of the initial free-induction decay. Fortunately, extrapolating the slow decay of the shortest τ echo train back to $2n\tau = 0$ provides a good estimate of the initial amplitude for all of the echo train decays. The initial point obtained in this way was added to each of the decay data sets for a given sample before fitting.

It was found that the distribution of slow motions in a given sample could be adequately approximated by assuming four discrete populations with correlation times ranging from close to the characteristic time of the quadrupole echo experiment $\left(\sim 10^{-5}\,\text{s}\right)$ to roughly four orders of magnitude longer. The precise way in which the continuous range of correlation times is binned into discrete values affects the magnitude of the population associated with each bin. As long as comparisons are based on fits using the same correlation-time bins, relative changes in the population magnitude associated with each bin can still give some indication of the extent to which changes in q-CPMG decay behavior reflect changes in the distribution of slow motions. The

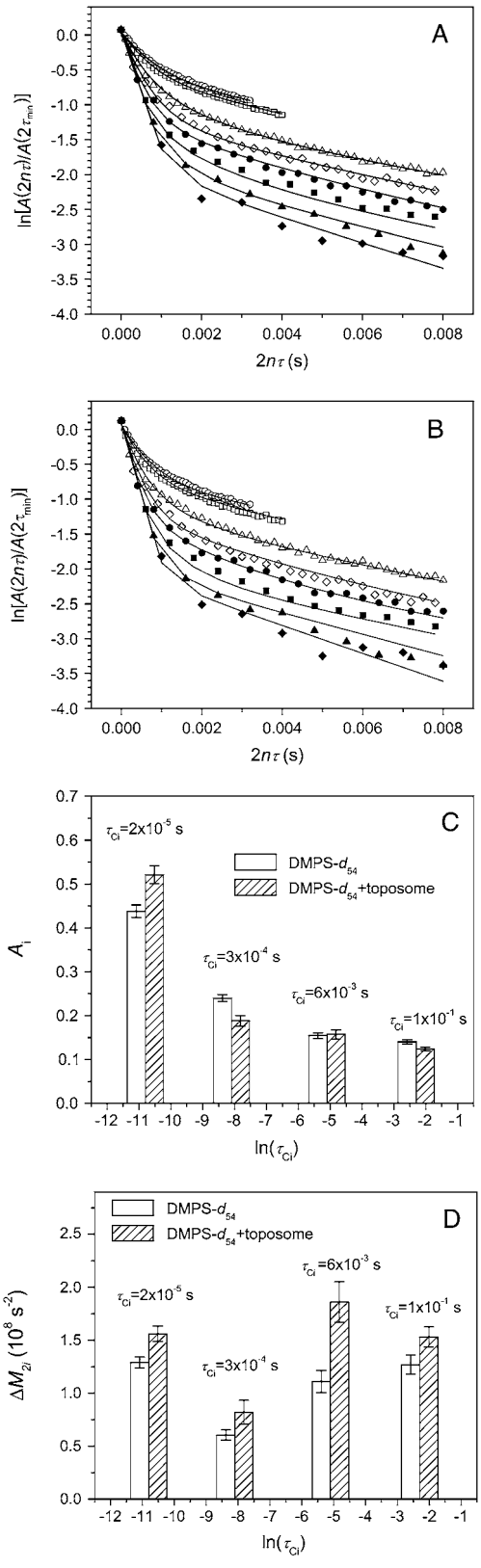

FIGURE 7 Results of simultaneously fitting q-CPMG decays for (*A*) DMPS-d_{54} and (*B*) DMPS-d_{54} plus toposome (lipid/protein = 80,000:1) in 100 μM Ca^{2+}. Symbols denote observed echo amplitudes for $\tau = 40\,\mu$s (○);$\tau = 50\,\mu$s(□);$\tau = 100\,\mu$s(8); $\tau = 150\,\mu$s(◇); $\tau = 200\,\mu$s(●); $\tau = 300\,\mu$s (■); $\tau = 400\,\mu$s (▲); and $\tau = 500\,\mu$s(♦). Solid lines are results of modeling the sample as four populations with different slow motions and a common fast motion. Parameters for the fits were obtained by minimizing χ^2 based on all datapoints and requiring that all parameters except τ be common to all decays for a given sample. Slow motion correlation times for the four populations were fixed at $\tau_{C1} = 2\times10^{-5}$ s, $\tau_{C2} = 3\times10^{-4}$ s, $\tau_{C3} = 6\times10^{-3}$ s, and $\tau_{C4} = 1\times10^{-1}$ s. (*C*) Comparison of the population magnitudes A_i obtained from the fit to DMPS-d_{54} echo-train decays (*open bar*) and the fit to echo decays for DMPS-d_{54} plus toposome (*shaded bars*). (*D*) Comparison of the second moments, ΔM_{2i}, of the quadrupole interaction modulation associated with the slow motion in each population obtained from the fit to DMPS-d_{54} echo-train decays (*open bar*) and the fit to echo decays for DMPS-d_{54} plus toposome (*shaded bars*). The contributions to the echo decay rate from common fast motions were $(1/T'_{2e}) = 76.3\,s^{-1}$ and $(1/T'_{2e}) = 72.9\,s^{-1}$ for DMPS-d_{54} and DMPS-d_{54} plus toposome, respectively.

discrete correlation times used here were $\tau_{C1} = 2\times10^{-5}$ s, a value slightly shorter than the smallest τ used in collection of the echo-train decays; $\tau_{C2} = 3\times10^{-4}$ s, a value of the order of the longest τ used; $\tau_{C3} = 6\times10^{-3}$ s, a value of about an order of magnitude larger than that of the longest τ used; and, $\tau_{C4} = 1\times10^{-1}$ s, a value much longer than the longest τ used.

Simultaneous fits to eight sets of $\ln[A(2n\tau)/A(2\tau_{min})]$ versus $2n\tau$ data corresponding to different values of τ for a given sample were thus carried out using Eq 3 to calculate $A(2n\tau)$ as a sum of four exponentials. The four correlation times, τ_{Ci} were fixed as described above. The nine remaining parameters were then varied to simultaneously minimize the discrepancy between the modeled decays and the eight decays observed for each sample. These nine fitting parameters comprise a population magnitude (A_i) for each of the four populations, a second moment (ΔM_{2i}) measuring the modulation of the interaction for each of the four populations, and a single decay rate $(1/T'_2)$ due to fast motions and assumed to be common to all four populations. In the calculation of χ^2 during the fitting procedure, each data point was weighted equally.

The results of the fitting procedure are shown in Fig. 7. The decays corresponding to the parameters obtained in the fit are shown as solid lines superimposed on the observed decays. The values of A_i and ΔM_{2i} corresponding to each of the selected correlation times are shown as bar graphs in the figure. Error bars shown are the standard errors in the fitted value of each parameter. Both fits gave similar values for the contributions to the echo decay rate from common fast motions. These were $(1/T'_2) = 76 \pm 3\,s^{-1}$ and $(1/T'_2) = 73 \pm 4\,s^{-1}$ for DMPS-d_{54} and DMPS-d_{54} plus toposome, respectively. As noted above, partitioning of the sample between populations corresponding to different slow motions is expected to depend on how the range of slow motion correlation times is sampled by the fixed times selected. In this case, the values of τ_{Ci}, selected to give roughly uniform intervals in the values of $\ln(\tau_{Ci})$, gave rise to a monotonic decrease in population from the shortest to the longest

correlation time for fits to both data sets. Toposome does not appear to change the population magnitudes for the slowest motions but does appear to induce a small shift from the second shortest correlation time to the shortest correlation time. This effect persists when the fit is redone with a slightly different set of fixed correlation times and might thus be of interest.

A more significant difference between the samples, though, is seen in the values of ΔM_{2i} obtained from the fits. Toposome appears to induce an increase in ΔM_{2i} for all populations. This likely accounts for the observed effect of toposome on quadrupole echo decay time in the liquid-crystalline phase. An increase in ΔM_{2i} for a given motion likely indicates a larger amplitude of reorientation. Possible interpretations include larger amplitude orientational fluctuations within the bilayer or larger amplitude undulations of the bilayer surface. Distortion of the surface due to local interaction with protein interacting at the surface might also increase ΔM_{2i} as long as diffusion of lipids through the region of local distortion is not constrained. In the case described here, any suggested interpretation must also be consistent with the lack of a significant observed perturbation of lipid acyl chain order or bilayer phase behavior by toposome.

The data presented here define the nature of the association of toposome with the bilayer. The effects of toposome on bilayer lipid motion suggest that this protein interacts peripherally with the membrane. This interaction occurs in the presence of 100 μM calcium and is not further modulated by increased concentrations of this cation. These results correlate well with those from a previous study in which we examined the effect of calcium on toposome structure (10). At concentrations of calcium <100 μM, apparent $k_d = 25$ μM, toposome underwent a change in secondary structure that facilitated binding to the bilayer. At higher concentrations of calcium, apparent $k_d = 240$ μM, toposome underwent a change in tertiary structure that enabled this protein to drive membrane-membrane adhesive interactions. The NMR study reported here clearly demonstrates that the calcium-induced tertiary structural change in toposome does not modulate protein-membrane interaction and thus more likely facilitates interaction between toposome molecules on opposing cell membranes, a reaction occurring at the cell surface. Collectively, these studies provide a mechanistic basis for the known cell-cell adhesive activity of toposome in the sea urchin embryo.

The patch hypothesis has been advanced as a model to explain the ability of sea urchin eggs to repair lesions in their plasma membrane (14,15). This model builds on the observation that yolk granules fuse into large vesicles when exposed to millimolar amounts of calcium. The large vesicles may then fuse with and reseal the plasma membrane. We have previously provided evidence that toposome associates peripherally with the outer surface of the yolk granule membrane (9) as follows.

1. Toposome can be dissociated from isolated yolk granules with EGTA, resulting in the loss of calcium-dependent yolk granule aggregation. Readdition of purified toposome to the EGTA-treated granules reconstituted calcium-dependent aggregation.
2. Preincubation of purified toposome with antitoposome antibody resulted in the inability of added protein to reconstitute calcium-dependent aggregation in EGTA-treated yolk granules.
3. When purified yolk granules were preincubated with antitoposome antibody followed by assay for calcium-dependent aggregation, no aggregation occurred.

These data, along with results described here, suggest the intriguing possibility that toposome may be an important player on the pathway leading to plasma membrane repair. A lesion in the egg plasma membrane would result in an influx of sea water containing 10 mM calcium. This calcium would drive the tertiary structural change in toposome associated with the yolk granule membrane. A toposome-toposome interaction would then serve to juxtapose yolk granule membranes, which would subsequently fuse in a process driven by SNARE proteins (32).

The authors are grateful to Mark McDonald and Ian Skanes for assistance with aspects of the analysis.

This research was supported by grants from the Natural Sciences and Engineering Research Council to J.J.R. and M.R.M.

REFERENCES

1. Ichio, I., K. Deguchi, S. Kawashima, S. Endo, and N. Ueta. 1978. Water-soluble lipoproteins from yolk granules in sea urchin eggs. Isolation and general properties. *J. Biochem. (Tokyo)* 84:737–749.
2. Kari, B. E., and W. L. Rottmann. 1985. Analysis of changes in a yolk glycoprotein complex in the developing sea urchin embryo. *Dev. Biol.* 108:18–25.
3. Ozaki, H. 1980. Yolk proteins of the sand dollar *Dendraster execentricus*. *Dev. Growth Differ.* 22:365–372.
4. Harrington, F. E., and D. P. Easton. 1982. A putative precursor to the major yolk protein of the sea urchin. *Dev. Biol.* 94:505–508.
5. Kari, B. E., and W. L. Rottmann. 1980. Analysis of the yolk glycoproteins of the sea urchin embryo. *J. Cell Biol.* 87:144a. (Abstr.).
6. Malkin, L. I., J. Mangan, and P. R. Gross. 1965. A crystalline protein of high molecular weight from cytoplasmic granules in sea urchin eggs and embryos. *Dev. Biol.* 12:520–542.
7. Noll, H., V. Matranga, M. Cervello, T. Humphreys, B. Kuwasaki, and D. Adelson. 1985. Characterization of toposomes from sea urchin blastula cells: a cell organelle mediating cell adhesion and expressing positional information. *Proc. Natl. Acad. Sci. USA.* 82:8062–8066.
8. Matranga, V., B. Kuwasaki, and H. Noll. 1986. Functional characterization of toposomes from the sea urchin blastula embryos by a morphogenetic cell aggregation assay. *EMBO J.* 5:3125–3132.
9. Perera, A., P. Davis, and J. J. Robinson. 2004. Functional role of a high mol mass protein complex in the sea urchin yolk granule. *Dev. Growth Differ.* 46:201–211.
10. Hayley, M., A. Perera, and J. J. Robinson. 2006. Biochemical analysis of a Ca^{2+}-dependent membrane-membrane interaction mediated by the sea urchin yolk granule protein, toposome. *Dev. Growth Differ.* 48: 401–409.

11. Scott, L. B., P. S. Leahy, G. L. Decker, and W. J. Lennarz. 1990. Loss of yolk platelets and yolk glycoproteins during larval development of the sea urchin embryo. *Dev. Biol.* 137:368–377.

12. Mayne, J., and J. J. Robinson. 1998. The sea urchin egg yolk granule is a storage compartment for HLC-32, an extracellular matrix protein. *Biochem. Cell Biol.* 76:83–88.

13. Mayne, J., and J. J. Robinson. 2002. Localization and functional role of a 41 kDa collagenase/gelatinase activity expressed in the sea urchin embryo. *Dev. Growth Differ.* 44:345–356.

14. Terasaki, M., K. Miyake, and P. McNeil. 1997. Large plasma membrane disruptions are rapidly resealed by calcium-dependent vesicle-vesicle fusion events. *J. Cell Biol.* 139:63–74.

15. McNeil, P., S. S. Vogel, K. Miyake, and M. Terasaki. 2000. Patching plasma membrane disruptions with cytoplasmic membrane. *J. Cell Sci.* 113:1891–1902.

16. Laemmli, U. K. 1970. Cleavage of structural proteins during assembly of the head bacteriophage T4. *Nature (Lond.).* 272:680–685.

17. Davis, J. H., K. R. Jeffrey, M. Bloom, M. I. Valic, and T. P. Higgs. 1976. Quadrupole echo deuteron magnetic resonance spectroscopy in ordered hydrocarbon chains. *Chem. Phys. Lett.* 42:390–394.

18. Prosser, R. S., J. H. Davis, F. W. Dahlquist, and M. A. Lindorfer. 1991. ^{2}H nuclear magnetic resonance of the gramicidin A backbone in a phospholipid bilayer. *Biochemistry.* 30:4687–4696.

19. McCabe, M. A., and S. R. Wassall. 1995. Fast-Fourier-transform dePaking. *J. Magn. Reson. B.* 106:80–82.

20. Bloom, M., and E. Sternin. 1987. Transverse nuclear spin relaxation in phospholipid bilayer membranes. *Biochemistry.* 26:2101–2105.

21. Davis, J. H. 1983. The description of membrane lipid conformation, order and dynamics by ^{2}H-NMR. *Biochim. Biophys. Acta.* 737: 117–171.

22. Abragam, A. 1961. The Principles of Nuclear Magnetism. Oxford University Press, London, UK.

23. Pauls, K. P., A. L. MacKay, O. Söderman, M. Bloom, A. K. Tangea, and R. S. Hodges. 1985. Dynamic properties of the backbone of an integral membrane peptide measured by ^{2}H-NMR. *Eur. Biophys. J.* 12:1–11.

24. Bloom, M., and E. Evans. 1991. Observation of surface undulations on the mesoscopic length scale by NMR. *In* Biologically Inspired Physics. L. Peliti, editor. Plenum Press, New York, NY. 137–147.

25. Stohrer, J., G. Gröbner, D. Reimer, K. Weisz, C. Mayer, and G. Kothe. 1991. Collective lipid motions in bilayer membranes studied by transverse deuteron spin relaxation. *J. Chem. Phys.* 95:672–678.

26. Bloom, M., E. Evans, and O. G. Mouritsen. 1991. Physical properties of the fluid lipid-bilayer component of cell membranes: a perspective. *Q. Rev. Biophys.* 24:293–397.

27. Meier, P., E. Ohmes, and G. Kothe. 1986. Multipulse dynamic nuclear magnetic resonance of phospholipids membranes. *J. Chem. Phys.* 85: 3598–3614.

28. Simatos, G. A., K. B. Forward, M. R. Morrow, and K. M. W. Keough. 1990. Interaction between perdeuterated dimyristoylphosphatidylcholine and low molecular weight pulmonary surfactant protein SP-C. *Biochemistry.* 29:5807–5814.

29. Dico, A. S., J. Hancock, M. R. Morrow, J. Stewart, S. Harris, and K. M. W. Keough. 1997. Pulmonary surfactant protein SP-B interacts similarly with dipalmitoylphosphatidylglycerol and dipalmitoylphosphatidylcholine in phosphatidylcholine/phosphatidylglycerol mixture. *Biochemistry.* 36:4172–4177.

30. Blicharski, J. S. 1986. Nuclear-spin relaxation in the presence of Mansfield-Ware-4 multipulse sequence. *Can. J. Phys.* 64:733–735.

31. Fiech, D. C., B. B. Bonev, and M. R. Morrow. 1998. Effect of pressure on dimyristoylphosphatidylcholine headgroup dynamics. *Phys. Rev. E.* 57:3334–3343.

32. Steinhardt, R. A., G. Bi, and J. M. Alderton. 1994. Cell membrane resealing by a vesicular mechanism similar to neurotransmitter release. *Science.* 263:390–393.